

# BEYOND NEAREST NEIGHBOR INTERPOLATION IN DATA AUGMENTATION

*Olivier Rukundo*

Department of Electronic and Computer Engineering,  
University of Limerick

## ABSTRACT

Avoiding the risk of undefined categorical labels using nearest-neighbor interpolation overlooks the risk of exacerbating pixel-level annotation errors in data augmentation. To simultaneously avoid these risks, the author modified convolutional neural networks' data transformation functions by incorporating a modified geometric transformation function to improve the quality of augmented data by removing the reliance on nearest-neighbor interpolation and integrating a mean-based class filtering mechanism to handle undefined categorical labels with alternative interpolation algorithms. Experiments on semantic segmentation tasks using three medical image datasets demonstrated both qualitative and quantitative improvements with alternative interpolation algorithms.

*Index Terms*— *interpolation, data augmentation, convolutional neural network, geometric transformation, pixel-level annotation, semantic segmentation*

## 1. INTRODUCTION

Data augmentation operation involves many techniques that operate at the data level rather than at the convolutional neural network (CNN) architectural level [1]. In the context of semantic segmentation with deep learning, this operation aims at increasing both training sets images and corresponding masks to help the CNN architecture of interest to generalize or perform better [1]. As of today, data augmentation still relies on traditional interpolation algorithms to increase or augment training sets through geometric transformations. The most popular interpolation algorithm used to avoid the risk of undefined categorical labels during these transformations is nearest-neighbor interpolation. This non-extra pixel interpolation (NPI) category algorithm is, specifically and routinely, used or leveraged for handling categorical labels in built-in functions commonly found in MATLAB or Python libraries [2], [3], [4]. However, there is no justification for neglecting the risk of pixel-level annotation error exacerbation instead of addressing both pixel-level annotation error exacerbation and undefined categorical label risks simultaneously. Note that, the inherent flaw of nearest neighbor interpolation's reliance on rounding functions leads to heavy jagged edge artifacts [4], [5] which results in mismatches between class boundaries and object boundaries once used for approximation purposes, ultimately, exacerbating pixel-level annotation errors. Also, note that completely avoiding pixel-level annotation errors is inherently challenging, as not all edge lines are defined by sharp transitions, and annotation tools rely on manual contour refinement to achieve pixel-perfect object

annotations [6]. In recent studies [2], [3], the author demonstrated that the use of extra pixel interpolation (EPI) algorithms or alternative interpolation algorithms, such as bicubic, bilinear, etc., for handling categorical labels could yield superior performance of the deep learning architecture of interest, thus opening new research focus on interpolation application. However, in [2], [3], the author did not evaluate effects of EPI algorithms in the context of data augmentation. To the best of the author's knowledge, there are currently no studies that simultaneously avoided previously mentioned risks or investigated EPI algorithms in handling categorical labels in data augmentation operations. In earlier studies, the nearest neighbor interpolation proved to produce jagged edge artefacts in the object's contours or edges of output or interpolated images [5], [7], [8]. This means that, for any approximation tasks during geometric transformation, the nearest neighbor interpolation algorithm will produce edge artefacts. In this way, the nearest neighbor interpolation algorithm will significantly exacerbate pixel-level annotation errors thus reducing the data augmentation quality, which also reduces the performance of deep learning architectures, as a result. To mitigate all these risks simultaneously, we simply updated convolutional neural networks' data transformation functions on which data augmentation operations rely, as explained in the following sections.

## 2. MATERIALS AND METHODS

### A. Datasets

Three datasets were downloaded from Kaggle, a large platform hosting community-shared models, datasets, and codes [9]. While selecting these datasets, the author focused on the diversity in digital imaging modalities and task of interest. The first dataset consists of fifty-five histology breast light-microscopy images and their corresponding masks. The second dataset includes fifty-five Magnetic Resonance Imaging (MRI) brain images and corresponding masks [10]. Lastly, the third dataset contains fifty-five colon polyp images, and their corresponding masks obtained through capsule endoscopy [11]. The choice of these fifty-five pairs of images and masks was imposed by balanced experimentation and computational resource constraints. Figure 1 shows a few samples of those images and masks pairs from these datasets. Here, it is important to note that, for CNNs' training purposes, all these images and masks were resized to  $256 \times 256$  due to documented benefits of training a CNN on images and masks of this size [2]. In the same context, note that each dataset was split into training set (70%), validation set (15%) & test set (15%).

### B. Convolutional Neural Networks

In this work, three convolutional neural network (CNN) architectures were used: U-Net [12], SegNet [13] and DeepLabV3+ [14]. The choice of these CNNs was based on their availability in popular software libraries, especially MATLAB.

Here, U-Net and SegNet network architectures were used with encoder depth set to four and convolutional layer filter size set to seven (others remained in default settings). Also, DeepLabV3+ network architecture, available in R2023b MATLAB, its first convolutional layer was updated to also accept a 1-channel input for grayscale training set (the rest remained in default settings).

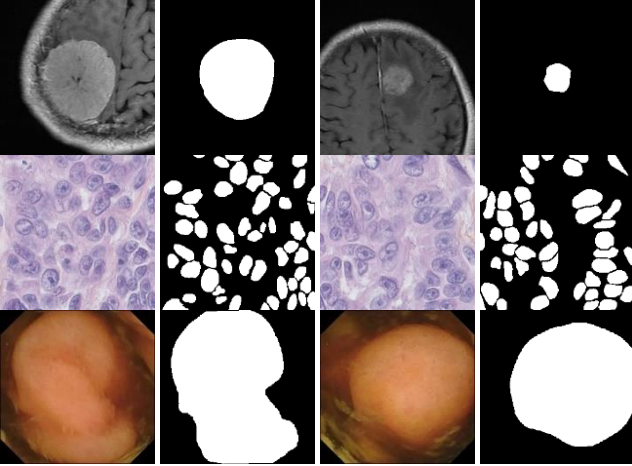


Figure 1: Top row: MRI brain image and mask pairs. Middle row: Microscopic histology breast image and mask pairs. Bottom row: Capsule endoscopy polyp image and mask pairs.

In this context, base architectures of interest, used in DeepLabV3+, were ResNet50, MobileNetV2, and ResNet18. However, experimental results obtained using ResNet50 were included in this work, primarily due to its superior performance compared to the results from other two base-architectures.

Hyperparameters relevant to these CNNs' architectures were set to meet the performance requirements, specifically epochs = 30, ADAM as optimizer, initial learning rate = 0.0001, batch size = 2, L2 regularization = 0.000005. NVIDIA's GeForce RTX3070 graphic card equipped computer was used for training purposes.

### C. Proposed Functions for Categorical Data Handling

The traditional version of the data augmentation or transformation function is shown in Figure 2 (top). In this case, when it comes to handling categorical labels, this function leverages the geometric transformation function (*imwarp*) with its routinely imposed nearest neighbor interpolation algorithm. Given risks associated with the nearest neighbor interpolation mentioned earlier, a modified version, taking also into account the pixel-level annotation error exacerbation risk, was developed as shown in Figure 2 (bottom).

As can be seen, in Figure 2 (bottom), the mapping operations were straight forward for converting categorical labels to their

corresponding pixels values or vice versa. When it comes to the modification of the *imwarp* function, only lines imposing the nearest neighbor interpolation algorithm were commented, to allow the use of an EPI algorithm. Due to the risk of producing undesired pixels when EPI algorithms are used for handling class pixels from categorical label mapping shown in Figure 2 (bottom), a filtering mechanism was proposed to remove this risk thus preventing the occurrence of undefined categorical labels at the end of the transformation.

In the recent past, the undesired pixel filtering mechanism was developed and applied externally before the training set content was fed to the CNN of interest, during multiclass semantic segmentation tasks [2], [3]. Here, the author internally integrated the undesired pixel filters mechanism to make the filtering process part of the augmentation process, during binary class semantic segmentation tasks. For simplicity purposes, the author developed a mean-based filtering mechanism, dubbed *global filter (GF)*, which leverages the Eq.1, Eq.2 and Eq.3 to filter the entire *modified-imwarp* function transformed mask.

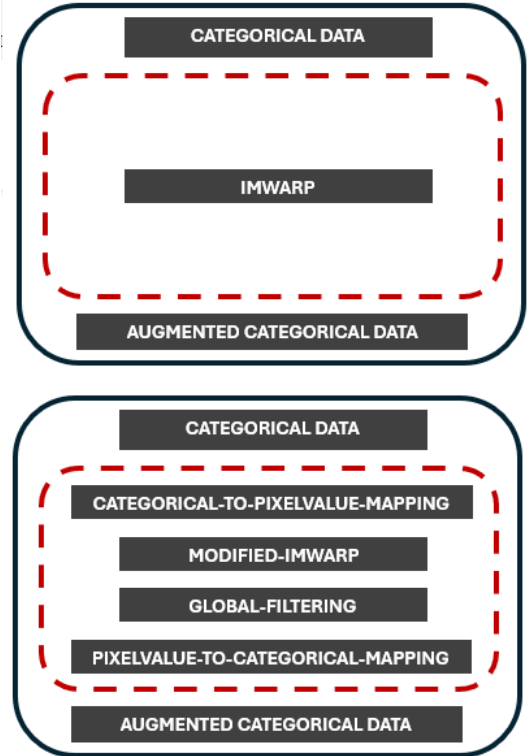


Figure 2: Comparison between the traditional and proposed functions for categorical data handling: Top: Traditional function that relies on NPI algorithms. Bottom: Proposed function that leverages EPI algorithms.

$$GF(x, y) = P(x, y), \quad \text{if } P(x, y) = 0 \mid P(x, y) = 255 \quad (1)$$

$$GF(x, y) = 255, \quad \text{if } P(x, y) > \mu \quad (2)$$

$$GF(x, y) = 0, \quad \text{if } P(x, y) \leq \mu \quad (3)$$

where, 0 and 255 are two-pixel classes corresponding to each categorical label;  $\mu$  is the 'mean' of all pixel values in the modified-imwarp function transformed mask ( $P$ );  $x$  and  $y$  are

coordinates of each pixel in  $P$  and  $GF$ .

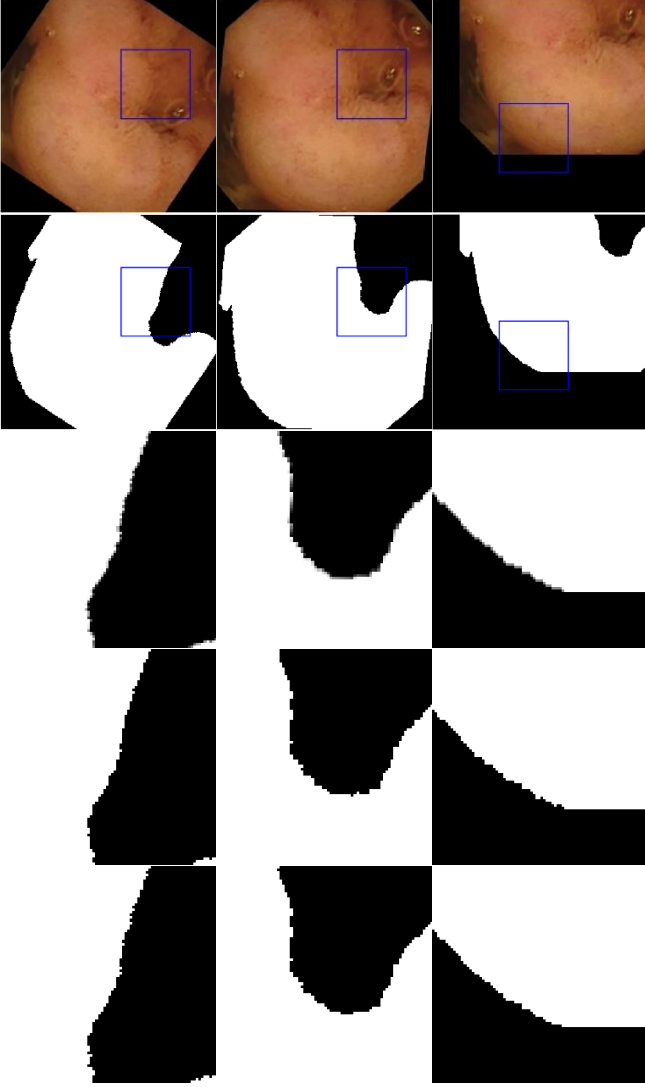


Figure 3: These three columns show rotated images and masks with cropped regions of interest. The third row shows an example of the modified-imwarp function output, while the fourth and fifth rows show the impact of GF and nearest-neighbor interpolation, respectively.

Figure 2's 4<sup>th</sup> row images show the effects of the *global filter* when an EPI algorithm (e.g., bicubic interpolation) was used to rotate, shear, and translate colon polyp modified-imwarp function transformed masks. Figure 2's 3<sup>rd</sup> row images show the effects of EPI algorithm, without the *global filter*. Figure 2's 5<sup>th</sup> row images show the effects of NPI algorithm, which does not require filtering. Now, in terms of columns, Figure 2's 1<sup>st</sup> and 2<sup>nd</sup> rows show rotated, sheared, and translated capsule endoscopy's Colon images and their corresponding ground truths, respectively. Here, the blue rectangle shows area to be cropped for better edge outline details visibility or visualization purposes. It is important to note that, the following were transformations and ranges used in each architecture stated earlier.

- $xTranslationRange = [-10 \ 10]$
- $yTranslationRange = [-10 \ 10]$

- $RangeOfHorizontalShear = [-15 \ 15]$
- $RangeOfVerticalShear = [-15 \ 15]$
- $RangeOfRotation = [-45 \ 45]$
- $RangeOfUniformScaling = [0.8 \ 1.2]$
- $brightnessFactor = 0.9:0.05:1.1$

Here, it is important to note that the brightness Factor only applies to images, not to masks. Also, note that these ranges were chosen without specific constraints but within reasonable limits.

### 3. EXPERIMENTAL RESULTS

#### A. Selected Evaluation Metrics

To evaluate the quality of predictions made by CNN architectures under various interpolation settings, *Accuracy* (Eq. 4), *IoU* (Eq. 5), and *meanBFScore* (Eq. 6 and Eq. 7), as well as the *Dice score* (Eq. 8), were used. These metrics were chosen due to their well-established suitability for assessing segmentation with deep learning. Here, True Positive (TP) refers to predicted pixels that overlap with ground truth pixels. False Positive (FP) refers to predicted pixels that do not overlap with ground truth pixels, while False Negative (FN) refers to ground truth pixels that were not predicted. As shown in [15], *Precision* and *Recall* can be calculated using TP, FP, and FN.

$$Accuracy\ score = \frac{TP}{TP+FN} \quad (4)$$

$$IoU\ score = \frac{TP}{TP+FP+FN} \quad (5)$$

$$BF1\ score = \frac{2*Precision*Recall}{Recall+Precision} \quad (6)$$

$$meanBFScore = \frac{1}{C} \sum_{i=1}^C BF1Score_i \quad (7)$$

where  $F1_i$  is the F1 score for class  $i$ , and  $C$  is the number of classes. Each class's *Precision* and *Recall* are calculated separately, then averaged.

$$Dice\ score = \frac{2*TP}{2*TP+FP+FN} \quad (8)$$

#### B. Evaluation by Sums of Ranks of Metric Scores

The idea of using ranks of metric scores instead of raw scores stemmed from statistical test concepts [16]. In this work, it was adopted to simplify the visualization of small differences among scores over the range of 0 to 1, once generated by the metrics mentioned in Section A. The highest raw score was given the rank 1, the lowest raw score was given the rank 3. In other words, the small rank means the better performance. In addition, as can be seen in the figures, we used the sums of ranks to further simplify the evaluation process.

Figure 4, Figure 5, and Figure 6 show different metric rankings and the sum of ranks for various interpolation configuration-based CNN architectures applied to three different datasets. Here, NEA\_NEA means that nearest neighbor algorithm was used to handle both images and masks. While

BIC\_BIC means that the bicubic interpolation algorithm was used to handle both images and masks. The other combination

includes the BIL abbreviation, which means the bilinear interpolation.

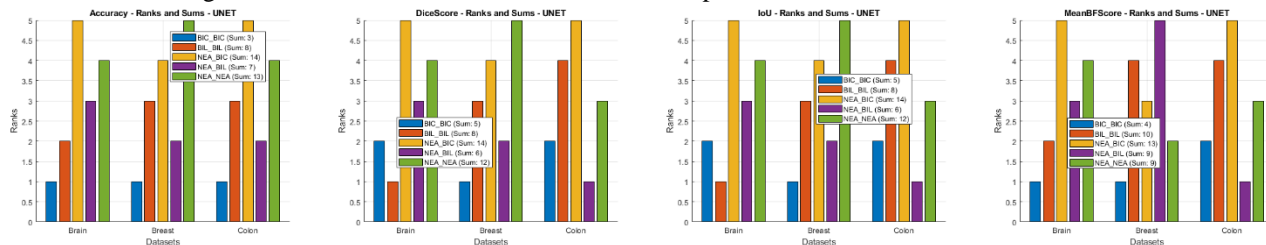


Figure 4: UNET: Accuracy, Dice, IoU and meanBFScore ranks

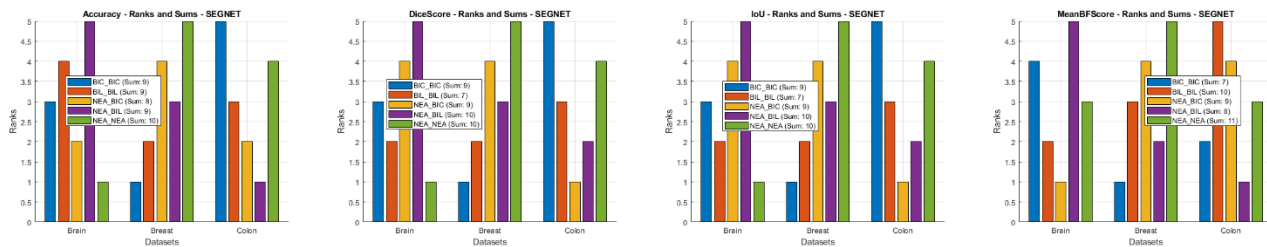


Figure 5: SEGNET: Accuracy, Dice, IoU and meanBFScore ranks

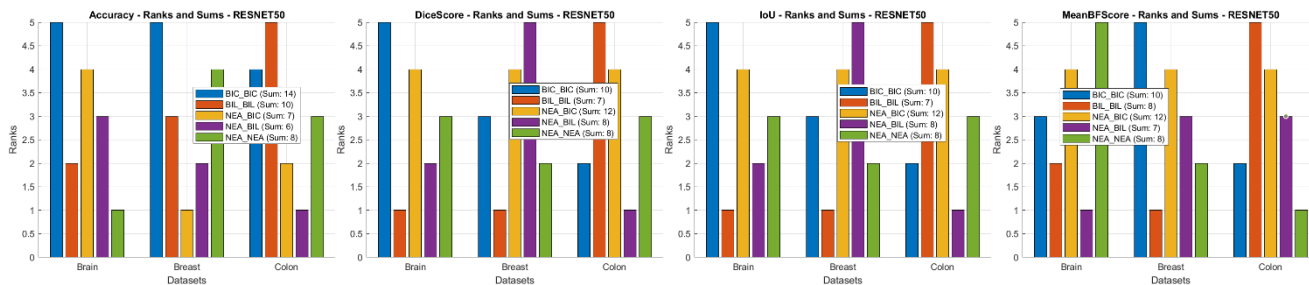


Figure 6: DEEPLAV3+R50: Accuracy, Dice, IoU and meanBFScore ranks

### C. Statistical Analysis of Ranks using T-test

A two-sample test (*t-test*) was chosen because it returns a test decision for the null hypothesis. Here, the null hypothesis rejection is very important because it helps ensure the difference among raw scores did not happen by chance. Therefore, the t-test was applied ranks presented in Figure 4, Figure 5, and Figure 6 and results were presented in Table 1. Here, it is important to note that various significance levels were used due to their direct effects on the test decision related to rejecting or accepting the null hypothesis. Those used were  $\alpha = 0.05$ ,  $\alpha = 0.2$  and  $\alpha = 0.35$ , which correspond to 95%, 80% and 65% confidence levels, respectively. As shown in Table 1, a value of 1 indicates the rejection of the null hypothesis while 0 indicates a failure to reject the null hypothesis, in accordance with the significance level ( $\alpha$ ). Also, it is important to note that postprocessing was not used to refine segmentation results.

### D. Qualitative Evaluation of Segmentation Masks

Figure 7, Figure 8, and Figure 9 present the segmentation mask results obtained using UNET, SEGNET, and DEEPLAV3+ under BC and NEA interpolation configurations for three different medical imaging datasets: Brain, Breast, and Colon. To facilitate the presentation and

comparison of segmentation mask results, the first column displays the test images, while the second column contains the corresponding ground truth masks. The third and fourth columns show the segmentation results produced by the BC\_BC-based architecture and the NEA\_NEA-based architecture, respectively.

## 5. DISCUSSIONS

As can be seen in Figure 4, in terms of Accuracy, Dice score, IoU and meanBFScore metrics, the UNET's BIC\_BIC was ranked the first thus demonstrating consistent superiority. In Figure 5, in terms of Accuracy, Dice score, and IoU, the SEGNET's BIC\_BIC were not ranked the first, at the exception of meanBFScore. Finally, in Figure 6, in terms of all metrics, the DEEPLAV3+/RESNET50's BIC\_BIC and NEA\_NEA were not ranked first. This superiority - seen in cases where NEA\_NEA was not used or simply where NEA was combined with another EPI algorithm - shows that it is irrational to ignore the risk of NEA's exacerbation of pixel-level annotation errors. Therefore, the proposed functions that allow the use of EPI algorithms must be considered as it simultaneously handles all risks previously mentioned.

Table 1:T-test results at different significance levels

Metrics	Methods	Models	p-value	h-value ( $\alpha = 0.05$ )	h-value ( $\alpha = 0.2$ )	h-value ( $\alpha = 0.35$ )
IoU	NEA_NEA / BIC_BIC	DeepLab/R50	0.5185	0.0000	0.0000	0.0000
		SEGNET	0.8512	0.0000	0.0000	0.0000
		UNET	0.0249	<b>1.0000</b>	<b>1.0000</b>	<b>1.0000</b>
	NEA_NEA / BIL_BIL	DeepLab/R50	0.8203	0.0000	0.0000	0.0000
		SEGNET	0.4676	0.0000	0.0000	0.0000
		UNET	0.2746	0.0000	0.0000	<b>1.0000</b>
	NEA_NEA / NEA_BIC	DeepLab/R50	0.0161	<b>1.0000</b>	<b>1.0000</b>	<b>1.0000</b>
		SEGNET	0.8416	0.0000	0.0000	0.0000
		UNET	0.3739	0.0000	0.0000	0.0000
	NEA_NEA / NEA_BIL	DeepLab/R50	1.0000	0.0000	0.0000	0.0000
		SEGNET	1.0000	0.0000	0.0000	0.0000
		UNET	0.0705	0.0000	<b>1.0000</b>	<b>1.0000</b>
Accuracy	NEA_NEA / BIC_BIC	DeepLab/R50	0.1012	0.0000	<b>1.0000</b>	<b>1.0000</b>
		SEGNET	0.8512	0.0000	0.0000	0.0000
		UNET	0.0006	<b>1.0000</b>	<b>1.0000</b>	<b>1.0000</b>
	NEA_NEA / BIL_BIL	DeepLab/R50	0.6213	0.0000	0.0000	0.0000
		SEGNET	0.8149	0.0000	0.0000	0.0000
		UNET	0.0241	<b>1.0000</b>	<b>1.0000</b>	<b>1.0000</b>
	NEA_NEA / NEA_BIC	DeepLab/R50	0.8025	0.0000	0.0000	0.0000
		SEGNET	0.6530	0.0000	0.0000	0.0000
		UNET	0.5185	0.0000	0.0000	0.0000
	NEA_NEA / NEA_BIL	DeepLab/R50	0.5614	0.0000	0.0000	0.0000
		SEGNET	0.8512	0.0000	0.0000	0.0000
		UNET	0.0132	<b>1.0000</b>	<b>1.0000</b>	<b>1.0000</b>
meanBFScore	NEA_NEA / BIC_BIC	DeepLab/R50	0.6779	0.0000	0.0000	0.0000
		SEGNET	0.2943	0.0000	0.0000	<b>1.0000</b>
		UNET	0.0668	0.0000	<b>1.0000</b>	<b>1.0000</b>
	NEA_NEA / BIL_BIL	DeepLab/R50	1.0000	0.0000	0.0000	0.0000
		SEGNET	0.7780	0.0000	0.0000	0.0000
		UNET	0.7247	0.0000	0.0000	0.0000
	NEA_NEA / NEA_BIC	DeepLab/R50	0.3295	0.0000	0.0000	<b>1.0000</b>
		SEGNET	0.6087	0.0000	0.0000	0.0000
		UNET	0.2051	0.0000	0.0000	<b>1.0000</b>
	NEA_NEA / NEA_BIL	DeepLab/R50	0.8203	0.0000	0.0000	0.0000
		SEGNET	0.5072	0.0000	0.0000	0.0000
		UNET	1.0000	0.0000	0.0000	0.0000
DiceScore	NEA_NEA / BIC_BIC	DeepLab/R50	0.5185	0.0000	0.0000	0.0000
		SEGNET	0.8512	0.0000	0.0000	0.0000
		UNET	0.0249	<b>1.0000</b>	<b>1.0000</b>	<b>1.0000</b>
	NEA_NEA / BIL_BIL	DeepLab/R50	0.8203	0.0000	0.0000	0.0000
		SEGNET	0.4676	0.0000	0.0000	0.0000
		UNET	0.2746	0.0000	0.0000	<b>1.0000</b>
	NEA_NEA / NEA_BIC	DeepLab/R50	0.0161	<b>1.0000</b>	<b>1.0000</b>	<b>1.0000</b>
		SEGNET	0.8416	0.0000	0.0000	0.0000
		UNET	0.3739	0.0000	0.0000	0.0000
	NEA_NEA / NEA_BIL	DeepLab/R50	1.0000	0.0000	0.0000	0.0000
		SEGNET	1.0000	0.0000	0.0000	0.0000
		UNET	0.0705	0.0000	<b>1.0000</b>	<b>1.0000</b>

In Table 1, looking at the UNET-based NEA\_NEA against UNET-based BIC\_BIC p-values and h-values, in terms of *IoU*, *Accuracy* and *Dice score*, there is rejection of null hypothesis at all levels of significance. In other networks and with some metrics, there is also rejection of null hypothesis but not all significant levels.

As can be seen, cases involving SEGNET and DEEPLABV3+ did not do always better than those involving UNET. In brief, this means that imposing the nearest neighbor interpolation algorithm by ignoring risk of exacerbating pixel-

level annotation errors is not rational, as there is a chance to improve the segmentation model's performance, when categorical labels are handled using the proposed functions that allow the use of EPI algorithms. Figure 7 shows the comparison of masks predicted by UNET-based BIC\_BIC and UNET-based NEA\_NEA. As can be seen, in all three dataset case images, the BIC\_BIC version produces textures and outlines that resemble more to the ground truth than the NEA\_NEA version. A similar situation is almost replicated in results shown in Figure 8 and Figure 9.

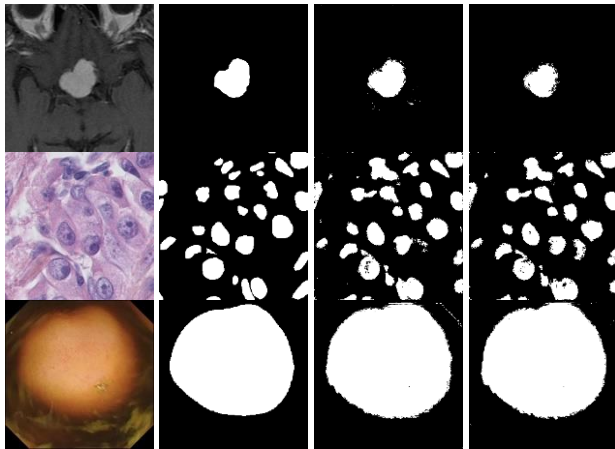


Figure 7: UNET: Left to right columns: Input image, ground truth, BC\_BC predicted mask, NEA\_NEA predicted mask. Top to bottom rows: Brain, Breast and Colon datasets.

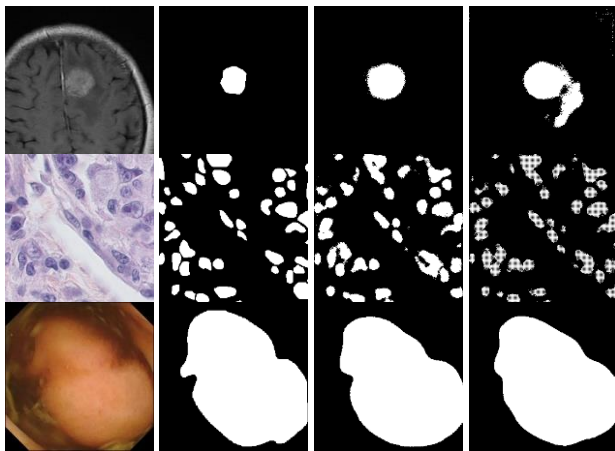


Figure 8: SEGNET: Left to right columns: Input image, ground truth, BC\_BC predicted mask, NEA\_NEA predicted mask. Top to bottom rows: Brain, Breast and Colon datasets.

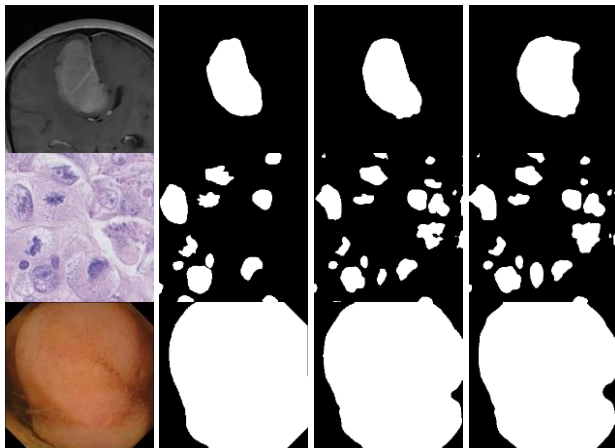


Figure 9: DEEPLABV3+/R50: Left to right columns: Input image, ground truth, BC\_BC predicted mask, NEA\_NEA predicted mask. Top to bottom rows: Brain, Breast and Colon datasets.

## 6. CONCLUSION

Simultaneously avoiding the risk of undefined categorical labels and risk of exacerbating pixel-level annotation errors in data augmentation is a way to go in efforts to improve the

quality of augmented data as demonstrated in this work. It was also demonstrated that only imposing nearest-neighbor interpolation for handling categorical labels in data augmentation tasks weakens the deep learning process, as it exacerbates pixel-level annotation errors and produces artifacts, negatively impacting the performance of deep learning architectures. By employing extra-pixel interpolation (EPI) algorithms, improvements in trained models' performance metrics such as accuracy, Dice score, and IoU were observed across multiple architectures and datasets. Note that, although created datasets were modestly sized, due to computational constraints, the proposed functions for categorical data handling remained a choice and can work with other architectures and datasets, which the author aims to explore in future work.

## 7. REFERENCES

- [1] Alomar K, Aysel HI, Cai X. Data Augmentation in Classification and Segmentation: A Survey and New Strategies. *J Imaging*. 2023 Feb 17;9(2):46. doi: 10.3390/jimaging9020046. PMID: 36826965; PMCID: PMC9966095.
- [2] Rukundo, O. Effects of Image Size on Deep Learning. *Electronics* 2023, 12, 985.
- [3] Rukundo, O. Evaluation of Extra Pixel Interpolation Algorithm with Interpolation Mask Processing for Medical Image Segmentation with Deep Learning. *SIViP* (2024).
- [4] Rukundo, O., Non-extra Pixel Interpolation, *International Journal of Image and Graphics*, 20(4), 2050031, 14 pages, 2020;
- [5] Rukundo, O., Evaluation of Rounding Functions in Nearest Neighbour Interpolation, *International Journal of Computational Methods*, 10 pages, 2021
- [6] Hollandi R, Diósi Á, Hollandi G, Moshkov N, Horváth P. AnnotatorJ: an ImageJ plugin to ease hand annotation of cellular compartments. *Mol Biol Cell*. 2020 Sep 15;31(20):2179-2186. doi: 10.1091/mbc.E20-02-0156. Epub 2020 Jul 22. PMID: 32697683; PMCID: PMC7550707.
- [7] Rukundo, O., Normalized Weighting Schemes for Image Interpolation Algorithms, *Applied Sciences*, 13(3):1741, 16 pages, 2023;
- [8] Rukundo, O., Schmidt, S., Stochastic Rounding for Image Interpolation and Scan Conversion, *International Journal of Advanced Computer Science and Applications*, 13(3), p. 13-22, 2022,
- [9] Kaggle Datasets < <https://www.kaggle.com/datasets> >, May 2023
- [10] Nikhil Tomar, Brain Tumor Segmentation, <<https://www.kaggle.com/datasets/nikhilroxtomar/brain-tumor-segmentation>>
- [11] Debesh Jha, KvasirCapsule-SEG (capsule endoscopy dataset): <https://www.kaggle.com/datasets/debeshjha1/kvasircapsuleseg>
- [12] Ronneberger, O.; Fischer, P.; Brox, T. U-Net: Convolutional networks for biomedical image segmentation. In *Medical Image Computing and Computer-Assisted Intervention—MICCAI 2015, Proceedings of the 18th International Conference, Munich, Germany, 5–9 October 2015*;
- [13] V. Badrinarayanan, A. Kendall and R. Cipolla, "SegNet: A Deep Convolutional Encoder-Decoder Architecture for Image Segmentation," in *IEEE Transactions on Pattern Analysis and Machine Intelligence*, vol. 39, no.12, pp. 2481-2495, 1 Dec. 2017
- [14] Chen, LC., Zhu, Y., Papandreou, G., Schroff, F., Adam, H. (2018). Encoder-Decoder with Atrous Separable Convolution for Semantic Image Segmentation. In: Ferrari, V., Hebert, M., Sminchisescu, C., Weiss, Y. (eds) *Computer Vision – ECCV 2018*. ECCV 2018. Lecture Notes in Computer Science, vol 11211. Springer, Cham.
- [15] Rukundo, O., Behonova, A., et al. Convolutional Neural Networks for Automatic Detection of Intact Adenovirus from TEM Imaging with Debris, Broken and Artefacts Particles: ArXiv: 2310.19630
- [16] Friedman, M. The Use of Ranks to Avoid the Assumption of Normality Implicit in the Analysis of Variance. *Journal of the American Statistical Association*, 32(200), 675–701, 1937